Constant-Power Performance and Plume Measurements of a Nested-Channel Hall-Effect Thruster

IEPC-2011-049

Presented at the 32nd International Electric Propulsion Conference,
Wiesbaden, Germany
September 11–15, 2011

Raymond Liang* and Alec D. Gallimore†
University of Michigan, Ann Arbor, MI, 48109, USA

The X2 nested-channel Hall-effect thruster has been operated at constant discharge powers of 5 kW and 6 kW. Thrust measurements showed that improved performance over an extended range of specific impulse can be obtained by transitions between operating modes of the X2. The simultaneous operation of both channels provided the best performance at low specific impulse, where higher mass flow rates were necessary to maintain total power. The inner channel provided optimal performance at high specific impulse, while the outer channel was best suited for the intermediate-I_{sp} region between the other two modes. Far-field RPA and E×B measurements were used to determine voltage utilization and charge utilization efficiencies during 6-kW operation. Discharge current measurements showed forms of interaction between discharge channels during simultaneous operation.

Nomenclature

I_d	= discharge current
$I_{d,AC}$	= AC component of discharge current
$I_{d,DC}$	= DC component of discharge current
I_{sp}	= specific impulse
$I_{sp,a}$	= anode specific impulse
$\dot{m}_a$	= anode mass flow rate
P_d	= discharge power
T	= thrust
V_a	= acceleration voltage
V_d	= discharge voltage
V_{mp}	= most-probable voltage
V_p	= plasma potential
Z	= charge state
η_a	= anode efficiency
η_q	= charge utilization efficiency
η_v	= voltage utilization efficiency
Ω	= ion species current fraction

*Ph.D. Candidate, Aerospace Engineering, rayliang@umich.edu.
†Arthur F. Thurnau Professor, Aerospace Engineering, alec.gallimore@umich.edu.

I. Introduction

The Plasmadynamics and Electric Propulsion Laboratory (PEPL) at the University of Michigan, through the support of the Michigan/Air Force Center of Excellence in Electric Propulsion, has developed and tested a laboratory-model nested-channel Hall-effect thruster (NHT) named the X2, as shown in Figure 1. This NHT was developed as a proof-of-concept demonstrator in order to determine the capabilities and operating characteristics of the nested-channel configuration. Through the use of three different exit areas, the X2 was designed to maintain constant discharge power over a wide range of specific impulse, I_{sp}, with particular emphasis on operation at low I_{sp} and high thrust-to-power ratio.

Nesting discharge channels is an alternate method of configuring high-power Hall thrusters in a manner that provides compact form factor and expanded capability. Past studies show that nesting channels can lead to significant reductions in thruster mass and footprint area when scaling to powers of 100 kW and greater.[1,2] With multiple combinations of active channels, NHTs have the ability to change exit area and therefore offer a form of variable-geometry Hall thruster. This capability also exists in clusters of Hall thrusters, but clusters are typically composed of multiples of the same thruster with the same exit area. Significantly larger variations in exit area can be achieved with fewer thrusters by nesting, as each additional channel must naturally increase in size. The concentric arrangement also keeps the thrust vector along the same axis regardless of the number of active channels and may therefore offer simpler thrust vector control compared to an equivalent cluster.

Multi-channel operation is one of the defining characteristics of NHTs and can be used to combine the capabilities of each individual channel to provide an extended operating envelope. NHTs could prove to be very adaptable in solar electric propulsion missions with large variations in available power, as the thruster could operate from the lowest power of the smallest channel to the highest power of all channels combined. The expanded mass flow rate capability of an NHT translates into a wider range of discharge currents and therefore allows power to be maintained across a broader spectrum of discharge voltages. As I_{sp} scales with discharge voltage, an NHT can use multi-channel operation to expand its specific impulse range at a given power level.

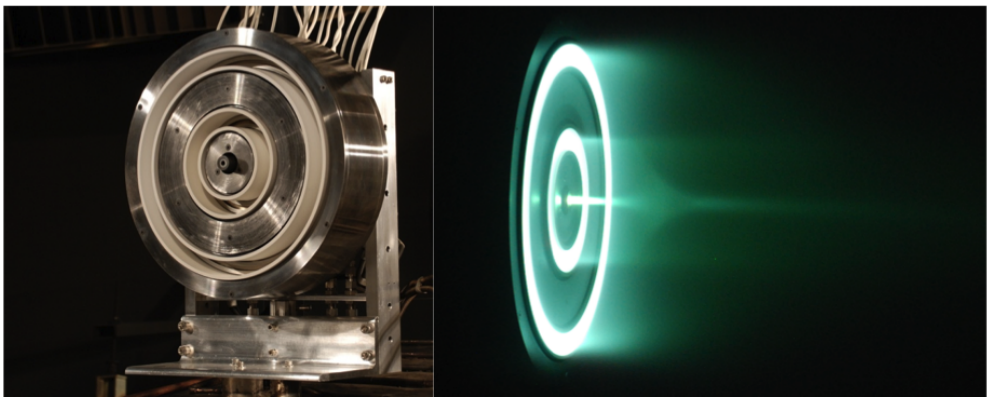

Figure 1: X2 nested-channel Hall-effect thruster

To investigate constant-power operation, the performance of the X2 was measured at discharge powers of 5 kW and 6 kW between discharge voltages of 125 V and 600 V. The throttling scheme used for these experiments is illustrated in Figure 2. Dual-channel mode, where both channels fire simultaneously, is used at low discharge voltages where high discharge currents and high mass flow rates are necessary. The X2 then transitions to the two single-channel modes with the outer channel by itself at medium discharge voltages and the inner channel by itself at high discharge voltages. Probe measurements were taken during the 6 kW operating conditions in order to observe variations in plume characteristics. Discharge current measurements at 200 kHz were also taken to monitor the temporal behavior of the thruster discharge.

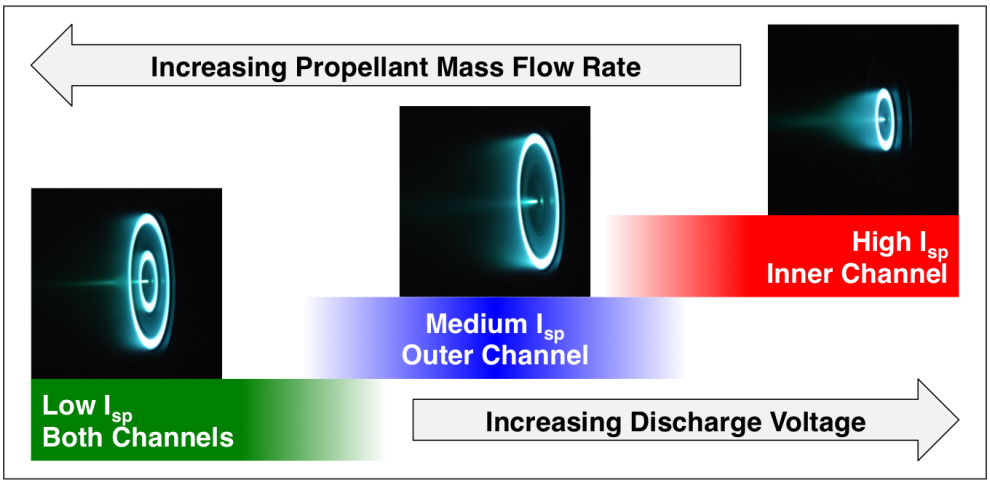

Figure 2: Constant power throttling scheme

II. Experimental Apparatus

A. Nested-Channel Hall-Effect Thruster

The X2 NHT features two discharge channels with similar cross-sectional dimensions, magnetic field designs, and gas distributors. During experimentation, the radial magnetic field pointed radially inward across the inner channel and radially outward across the outer channel. Testing of the X2 was conducted with an updated version of the internally-mounted LaB_6 hollow cathode used for a 6-kW laboratory Hall thruster. At the beginning of every pumpdown, both channels of the X2 were operated for a bake-out period of one hour.

Both anodes and the cathode had separate stainless steel propellant feed lines with viton isolators at the thruster. MKS Model 1179A mass flow controllers were used to regulate propellant flow through the outer anode and the cathode, and an MKS Model 1159B mass flow controller was used for the inner anode. All three mass flow controllers were connected to an MKS Model 247C 4-channel readout and calibrated using a constant volume method that included compressibility effects. The manufacturer-specified accuracy of the mass flow controllers is 1% of full scale. Research grade xenon at 99.999% purity was used throughout testing.

Electrical connections for the X2 were made such that each channel had a separate discharge power supply, and the common for both discharge circuits was connected to the shared internal cathode. This electrical configuration was based on previous work performed at PEPL on clustered Hall thrusters with a shared hollow cathode.[3,4] Operation of both channels of the X2 is also possible with a single, shared discharge power supply, as discussed briefly in the appendix of this paper. The thruster was electrically grounded to the facility ground during testing, and discharge voltages were measured from contacts at the back of the X2. Discharge current oscillations were measured using F.W. Bell NT-series current sensors placed in series with the anodes. Both current sensors were placed on the thruster side of a discharge filter that included two 220 μF capacitors in parallel with each discharge power supply.

The inner channel discharge was powered by a Sorensen PRO 600-16T while the outer channel discharge was powered by an American Reliance HPS 1000-100-K027. Power for the magnets were provided by three EMI EMS 60-10 power supplies and one EMI EMS 100-10. The two trim coils were powered by a Sorensen DCS 60-18E and a DCS 600-1.7. Cathode keeper power was provided by an EMI EMS 600-1.6, and heater power was provided by a Sorensen DCS 33-33.

B. Inverted Pendulum Thrust Stand

Thrust measurements were taken on an inverted-pendulum thrust stand designed by NASA Glenn Research Center.[5] Displacement of the thrust stand was measured using a Linear Variable Differential Transformer (LVDT) and was controlled by a single null coil powered by an Acopian A36MT230 power supply and a Trust Automation TA105 amplifier. Zero displacement was maintained by a Stanford Research Systems SIM960 PID controller. The LVDT and PID output signals were recorded on a Cole-Parmer K-80550-30 flatbed recorder.

Calibration of the thrust stand was performed before and after each day of performance testing. The calibration slope changed only by a fraction of a percent over the course of a day. The PID signal corresponding to zero thrust (the

"zero") was periodically measured by shutting off all power and propellant flow to the thruster. Thrust measurements were always taken between two zeros, where the change in zero was assumed to be linear with time. At the time of a particular operating condition, the zero-thrust reference voltage was determined by linear interpolation between two zeros. The instantaneous difference between the interpolated reference voltage and the PID output voltage was converted into thrust *a posteriori* using the thrust stand calibration.

C. E×B Probe

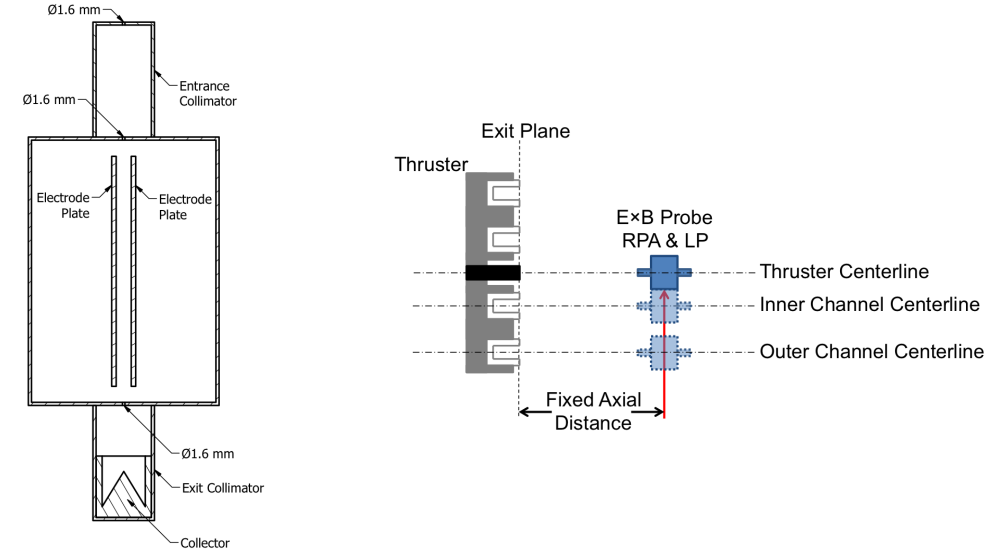

(a) E×B probe schematic (Not to scale)

(b) E×B probe, RPA, and LP actuation

Figure 3: E×B probe schematic and top view of actuation of E×B probe, RPA, and LP

The E×B probe used in this study was designed by NASA Glenn Research Center and is more thoroughly described in previous work by Reid *et al*.[6] The probe features a 150-mm test section with 75-mm entrance and exit collimators. Aperture diameters for the entrance orifice and the collimating orifices were all approximately 1.6 mm. The internal magnetic field was created by sintered hard ferrite permanent magnets, while the internal electric field was generated by a Keithley 2410 Sourcemeter via two parallel conducting plates. Ions that passed through the test section were collected by a cone-and-cylinder collector that has been spray coated with tungsten to reduce secondary electron emission. Collected current was measured by a Keithley 6485 Picoammeter.

D. Retarding Potential Analyzer

The RPA used in this study was originally designed and built by the Air Force Research Laboratory and is described in further detail in separate documents by Reid and Hofer.[7,8] The grids and the collector of the RPA are separated by macor spacers that are housed within a macor sleeve and stainless steel shell. In order to repel electrons, the electron repelling grid was biased to -30±0.1 V with respect to facility ground by an Kukusui PAD 110-1.5L power supply. The voltage applied to the ion retarding grid was swept relative to facility ground by a Keithley 2410 Sourcemeter, and the collected current was measured by a Keithley 6485 Picoammeter.

A cylindrical Langmuir probe was placed adjacent to the RPA for the necessary measurements of local plasma potential. The Langmuir probe was composed of a 0.25-mm diameter tungsten wire that protruded 5.7 mm from a 1.5-mm diameter alumina tube.

The E×B probe, RPA, and Langmuir probe were placed 2 m downstream of the exit plane to minimize probe heating and perturbations to the thruster. The E×B probe was protected by graphite plates in front and on the plume side to further prevent overheating of the probe body. The RPA was protected by a grafoil shutter and the shadow of the E×B probe when the probe array was not in use. Radial actuation was provided by a 1.5-m linear translation stage, allowing each of the probes to be placed directly downstream of the individual centerlines of the inner channel

and outer channel. The axial and lateral position uncertainties were both approximately ±10 mm due to slips in the positioning system.

E. Vacuum Facility

Experiments on the X2 were performed in the Large Vacuum Test Facility (LVTF) in PEPL at the University of Michigan. LVTF is a cylindrical vacuum chamber that measures 6 meters in diameter and 9 meters in length. Seven CVI model TM-1200 cryopumps with liquid nitrogen shrouds are used to achieve a base pressure of 3×10^{-7} torr. The nominal pumping speed for xenon is 245,000 l/s with all seven cryopumps operating. Pressure was measured using a Varian UHV-24 nude ionization gauge and a Varian model 571 Bayard-Alpert ionization gauge connected to a Varian XGS-600 gauge controller. The reported background pressures are an average of the pressure measurements taken by the two gauges. Typical accuracy for ionization gauges is approximately ±20% according to Varian.[9]

III. Results and Discussion

The settings used for the 5-kW and 6-kW operating conditions are shown in Table 1. For all dual-channel conditions, the discharge voltages were the same across both channels, and the division of propellant mass flow rates was held near a ratio of 2.4:1 between the outer channel and inner channel. Cathode flow fraction was held at 10% of the combined anode mass flow rate during the 6-kW operating conditions. This percentage has been used since the first dual-channel firings of the X2 and has consistently provided stable cathode operation. To investigate if the X2 would operate with less cathode flow, a decreased cathode flow fraction of 7% was used for the 5-kW operating conditions. Plume measurements were taken during operating conditions indicated in the last column of Table 1.

Controlling discharge power was performed by iterative adjustment of the magnetic field and mass flow rates at a fixed discharge voltage. Tuning of the electromagnets was done to maximize anode efficiency, as minima in the discharge current were not always found. Anode mass flow rates were adjusted to achieve the required discharge currents to maintain constant power. The cathode mass flow rate was always adjusted after the magnetic field and the anode flow rates in order to ensure continuously stable cathode operation. The cathode heater and keeper both remained shut off after ignition of the thruster and were not operated during this process.

Thrust measurements were used to determine anode efficiency, η_a, and anode specific impulse, $I_{sp,a}$. These parameters are defined in Equations 1 and 2.

$$\eta_a = \frac{T^2}{2\dot{m}_a P_d} \tag{1}$$

$$I_{sp,a} = \frac{T}{\dot{m}_a g} \tag{2}$$

Anode quantities are used instead of total quantities because no attempts were made to optimize cathode efficiency at each operating point due to time constraints. Additionally, discharge power, not total power, was held constant throughout these conditions, so the use of anode quantities is more suitable.

A. Performance Measurements

All performance data at 5 kW and 6 kW are compiled into Figures 4(a) and 4(b). These plots show the tradeoff between thrust and anode specific impulse while operating at constant discharge power. Discharge voltages are indicated for one operating condition of each mode for reference. The achieved thrust ranges were 245 mN - 397 mN at 5 kW and 282 mN - 460 mN at 6 kW. Uncertainty in the thrust measurements was ±3 mN and uncertainty in anode specific impulse typically did not exceed ±115 s. Anode efficiency was accurate to ±3% absolute.

Both sets of data reflect the throttling scheme shown in Figure 2 and illustrate the ability for an NHT to transition between modes in order to optimize performance and extend its specific impulse range. Dual-channel operation produced the best performance up to approximately 1600 s $I_{sp,a}$. The range over which the outer channel was best varied with the operating power. At 5 kW, the outer channel took over between 1600 s and 1800 s $I_{sp,a}$, and at 6 kW, this range expands to 1600 s to 2050 s. Beyond 1800 s - 2050 s $I_{sp,a}$, optimal performance was provided by the inner channel. At both 5 kW and 6 kW, the outer channel reached conditions where its thrust began to plateau or decrease with decreasing specific impulse. By transitioning to dual-channel mode for low specific impulse, the limitations of the outer channel were avoided. The use of both channels also provided $I_{sp,a}$ 1000 s below the lowest demonstrated $I_{sp,a}$ of the inner channel, as the dual-channel mode provided up to twice the highest mass flow rate of the inner channel.

Table 1: Constant-power throttling table

Discharge Voltage [V]	Anode Mass Flow Rate (Inner Channel) [mg/s]	Anode Mass Flow Rate (Outer Channel) [mg/s]	Background Pressure [torr-Xe]	Plume Measurements
6-kW Conditions				
125	12.0	29.6	2.7×10^{-5}	
150	11.0	27.1	2.4×10^{-5}	*
200	9.0	21.8	1.8×10^{-5}	*
250	7.5	18.3	1.6×10^{-5}	*
300	6.4	15.6	1.3×10^{-5}	
350	5.6	13.6	1.2×10^{-5}	
200	-	28.8	1.8×10^{-5}	*
250	-	25.4	1.6×10^{-5}	*
300	-	21.7	1.3×10^{-5}	*
350	-	18.9	1.2×10^{-5}	
400	-	16.8	1.0×10^{-5}	
300	18.0	-	1.1×10^{-5}	*
400	14.7	-	8.8×10^{-6}	*
500	12.3	-	7.3×10^{-6}	
600	10.2	-	6.1×10^{-6}	*
5-kW Conditions				
150	9.3	23.0	2.0×10^{-5}	
200	7.5	18.5	1.6×10^{-5}	
350	6.3	15.8	1.4×10^{-5}	
300	5.6	12.9	1.2×10^{-5}	
350	4.5	11.0	1.0×10^{-5}	
400	3.9	9.5	9.0×10^{-6}	
200	-	24.8	1.7×10^{-5}	
250	-	21.4	1.4×10^{-5}	
300	-	18.5	1.2×10^{-5}	
350	-	16.2	1.1×10^{-5}	
400	-	14.4	9.5×10^{-6}	
250	17.6	-	1.1×10^{-5}	
300	16.1	-	1.1×10^{-5}	
400	12.5	-	8.4×10^{-6}	
450	11.4	-	7.7×10^{-6}	
500	10.4	-	7.1×10^{-6}	
550	9.4	-	6.5×10^{-6}	
600	8.7	-	6.2×10^{-6}	

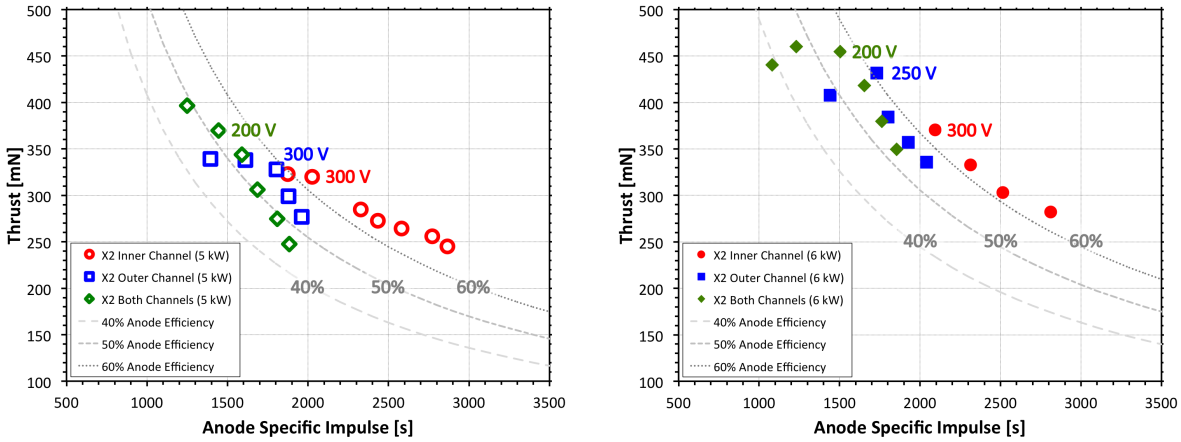

(a) 5 kW (b) 6 kW

Figure 4: Thrust as a function of anode specific impulse at constant discharge power

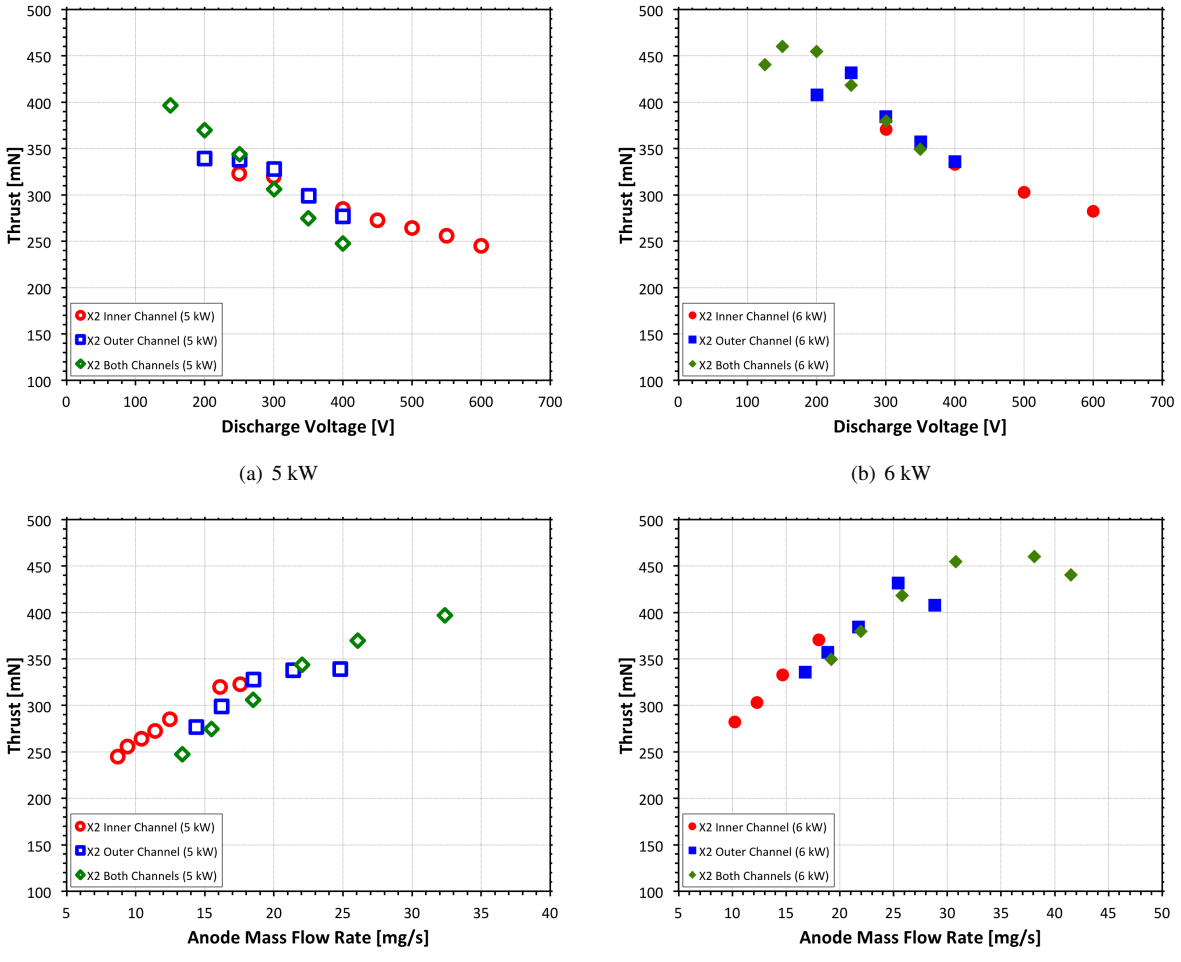

(a) 5 kW (b) 6 kW

(c) 5 kW (d) 6 kW

Figure 5: Measured thrust as a function of discharge voltage and anode mass flow rate at constant discharge power

To examine the variation of performance at constant power in greater detail, thrust can be examined as a function of the discharge voltage and anode mass flow rate. These parameters were chosen because they were directly adjusted by the operator, as opposed to parameters, such as discharge current, that were indirectly controlled. The reader should note that both V_d and $\dot{m}_a$ were adjusted simultaneously between operating conditions. Figures 5(a) and 5(b) show the measured thrust as a function of discharge voltage while Figures 5(c) and 5(d) show thrust as a function of anode mass flow rate.

The data in Figures 5(a)-5(d) provide a means of decomposing the operating ranges of each mode into discharge voltage and the corresponding mass flow rates. For constant-power operation, the dual-channel mode was well-suited for low discharge voltages up to 200 V - 250 V. The corresponding mass flow rates, which varied in magnitude based on the power, spanned the upper 44% of the 5-kW $\dot{m}_a$ range and the upper 50% of the 6-kW $\dot{m}_a$ range. The inner channel provided the best performance above 300 V - 400 V, covering the lower 38% and 28% of the $\dot{m}_a$ range at 5 kW and 6 kW, respectively. The intermediate discharge voltage and mass flow rates were covered by the outer channel.

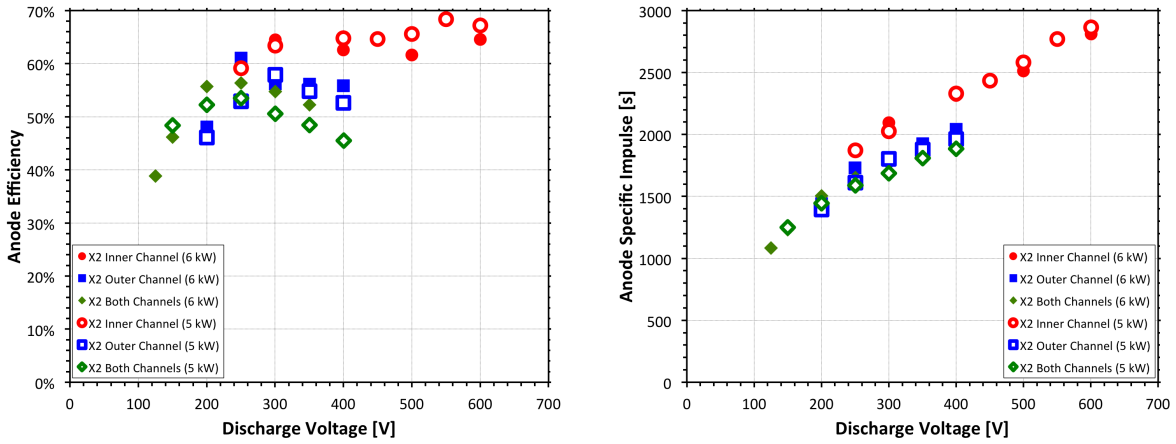

(a) Anode Efficiency

(b) Anode Specific Impulse

Figure 6: Anode efficiency and anode specific impulse as a function of discharge voltage at constant discharge power

Figures 6(a) and 6(b) show the anode efficiency and anode specific impulse for the 5-kW and 6-kW operating conditions. Anode efficiency varies from 39% to 68% while anode specific impulse varies from 1082 s to 2866 s. In general, the inner channel operates with the higher specific impulse than the other two modes of the X2, and therefore, it is particularly suited for high-voltage, high-I_{sp} operation. The inner channel is also more efficient, resulting in a small gap between the inner-channel and outer-channel curves in Figure 4(b).

The outer channel of the X2 is meant primarily to increase mass flow rate at low discharge voltages and does not operate the most efficiently at 300 V or above. This is most apparent in the 5-kW efficiency data, where the outer channel's anode efficiency decreases at 300 V and above. At 6 kW, η_a for the outer channel decreases from 250 V to 300 V and plateaus around 56%-58% up to 400 V. As the outer channel is dominant during dual-channel operation, efficiency of the dual-channel mode also decreases above 300 V. However, for more efficient operation, a transition can be made to the inner channel, which is meant for high-voltage operation.

B. Plume Measurements

Figure 7(a) shows the normalized derivatives of cubic-spline fits to RPA measurements taken during nine of the 6-kW operating points. RPA measurements were used to determine the most-probable voltage, V_{mp} and voltage utilization efficiency, η_v, as defined in Equation 3 and shown in Figure 8(a). The error in V_{mp} was estimated to be ±10 V based on existing analyses.[8,11] Plasma potential, V_p, was determined using a cylindrical Langmuir probe adjacent to the RPA. The characteristic knee between the transition and electron saturation regions in the measured I-V characteristics yielded V_p with a relative uncertainty of as high as ±50%.

$$\eta_v = \frac{V_a}{V_d} = \frac{V_{mp} - V_p}{V_d} \tag{3}$$

The E×B traces are shown in Figures 7(b) and 7(c) and were used to determine charge utilization efficiency, η_q, as

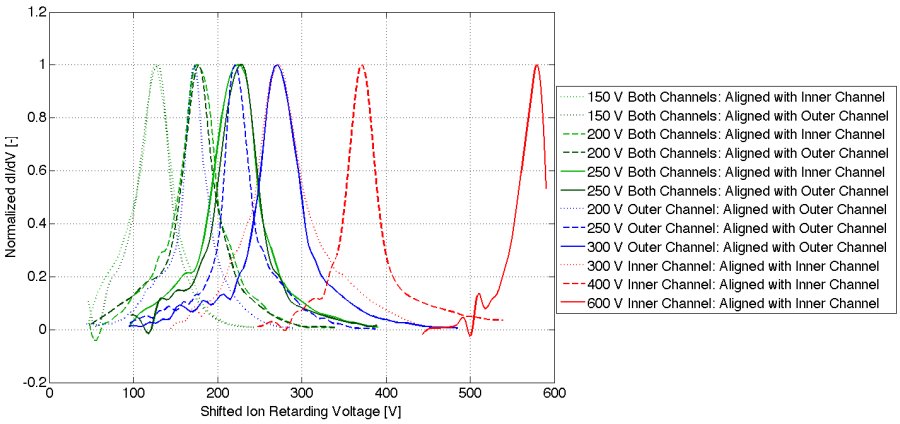

(a) RPA measurements

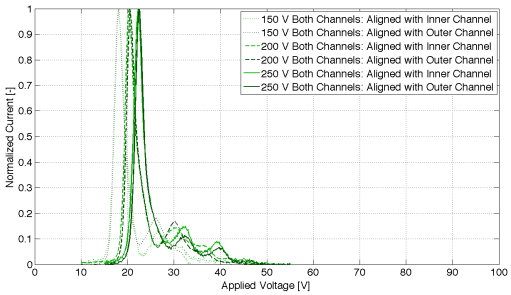

(b) Dual-channel E×B measurements

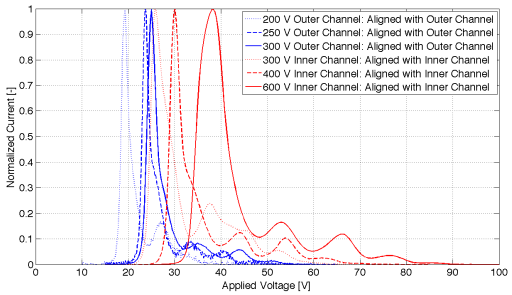

(c) Single-channel E×B measurements

Figure 7: RPA and E×B measurements at 6 kW

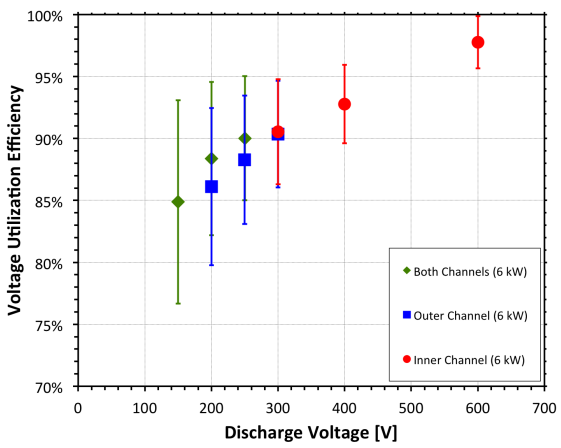

(a) Voltage Utilization

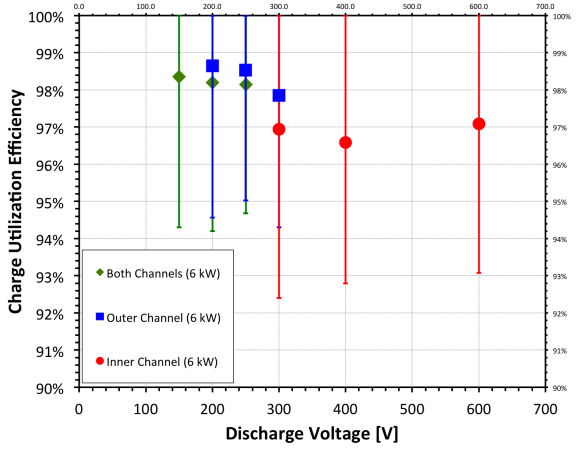

(b) Charge Utilization

Figure 8: Voltage utilization and charge utilization efficiencies at 6 kW

defined in Equation 4 and shown in Figure 8(b).

$$\eta_q = \frac{\left(\sum_{i=1}^{n} \frac{\Omega_i}{\sqrt{Z_i}}\right)^2}{\sum_i^n \frac{\Omega_i}{Z_i}} \tag{4}$$

The current fraction of the ith ion species, Ω_i, is determined from an E×B probe trace by the methods outlined by Shastry *et al.*[10] Specifically, the triangle method and simplified charge exchange model are used in this study to calculate Ω_i. Z_i is the ion charge state. Based on analysis by Shastry, the relative uncertainties associated with the current fractions were ±3% for singly-charged species and ±20% for multiply-charged species.

Dual-channel conditions at 150 V, 200 V, and 250 V each had two sets of RPA, Langmuir probe, and E×B measurements, as each probe was moved directly downstream of each channel. The ion retarding voltages are shifted according to the measured plasma potentials for each RPA trace such that the peaks correspond to the most-probable voltages.

While operating at constant power, V_{mp} of the X2 increased with increasing discharge voltage and decreasing mass flow rate. Variations in RPA traces between both channels in dual-channel mode were small and differences in V_{mp} fell within the error margin. The highest measured voltage utilization efficiency during 6 kW operation, as shown in Figure 8(a), was 98% at 600 V, and the lowest was 85% at 150 V. RPA data suggest that dual-channel mode may operate with slightly higher η_v than a single-channel mode at the same discharge voltage, as seen previously with the X2 up to 200 V.[12] However, the small differences in V_{mp} and η_v along with their uncertainties make this difference unresolvable and require additional probe measurements for a complete investigation.

Doubly- and triply-charged ions were detected in all dual-channel conditions, as previously seen in low-voltage, dual-channel measurements of the X2.[12] However, triply-charged species fractions during dual-channel conditions at 150 V, 200 V, and 250 V were 1% or less. Beginning at 300 V for both single-channel modes, E×B measurements began detecting quadruply-charged ions despite the decreasing mass flow rates with increasing discharge voltage. The quadruply-charged ion species fractions never exceeded 1% for all measurements taken. As shown in Figure 8(b), η_q did not vary significantly across all the 6-kW conditions and stayed within a 3% range. Despite having more multiply-charged species and therefore lower charge utilization efficiency, dual-channel mode still provided better performance than the outer channel at 200 V and below.

C. Discharge Current Measurements

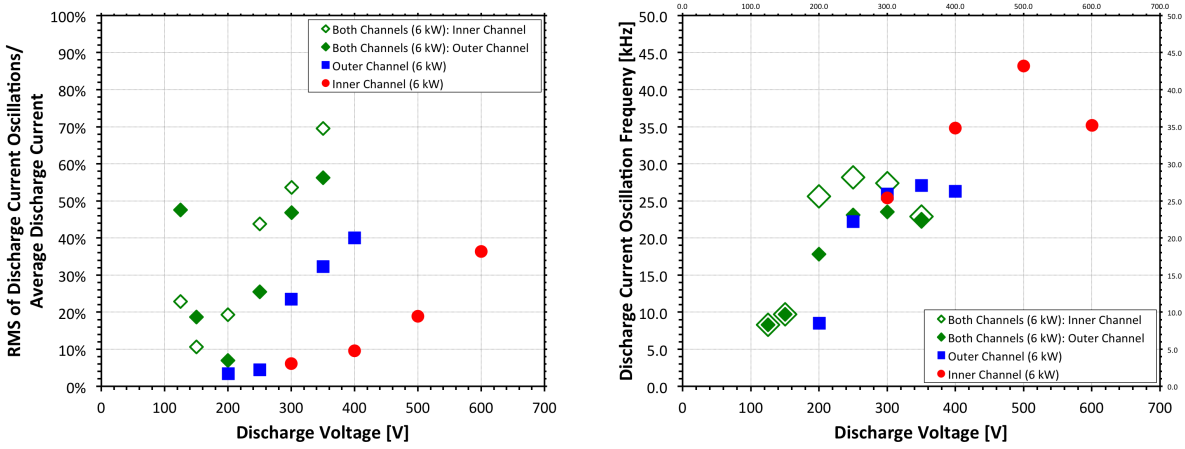

(a) Normalized RMS of $I_{d,AC}$

(b) Breathing mode frequency

Figure 9: Characteristics of the discharge current oscillations at 6 kW

Measurements of discharge current, I_d, were taken during 6-kW operation for each channel at 200 kHz with F.W. Bell NT-series magneto-resistive current sensors place in series with the anodes. Samples of the discharge currents in both time and frequency space are shown in Figures 10(a) - 10(f). To quantify the strength of oscillations, the RMS of the AC component of the discharge current, $I_{d,AC}$, was computed and expressed as a fraction of the DC component of the discharge current, $I_{d,DC}$, as shown in Figure 9(a). For dual-channel conditions, the two discharge currents were

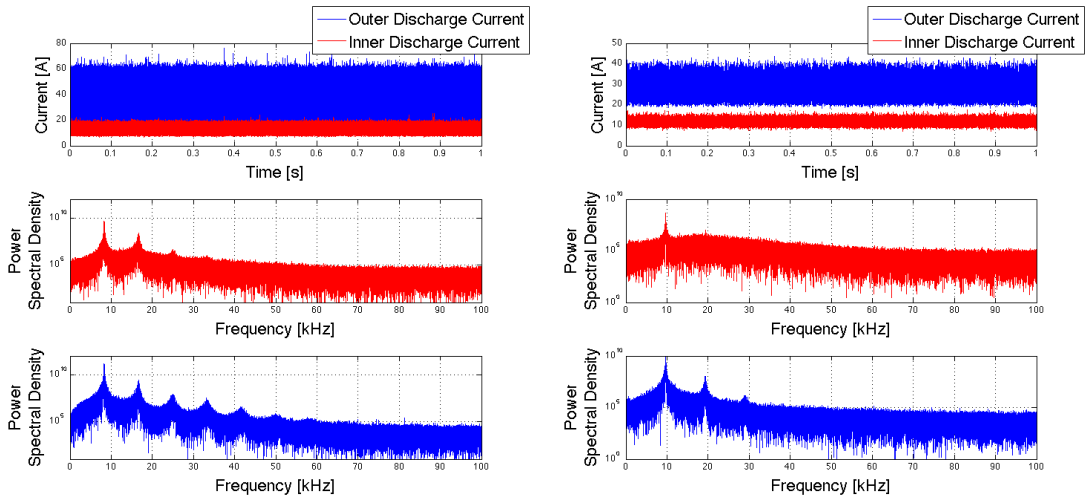

(a) 125 V

(b) 150 V

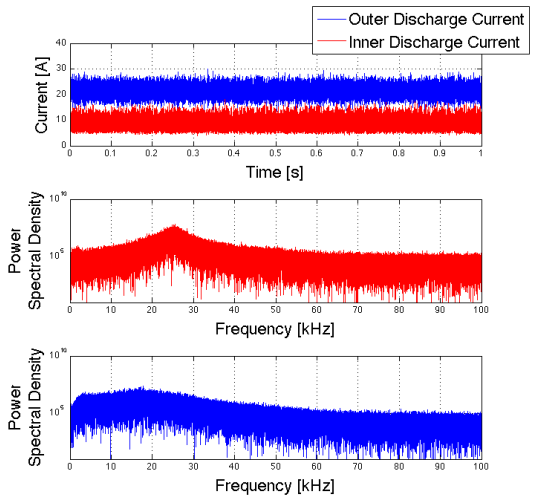

(c) 200 V

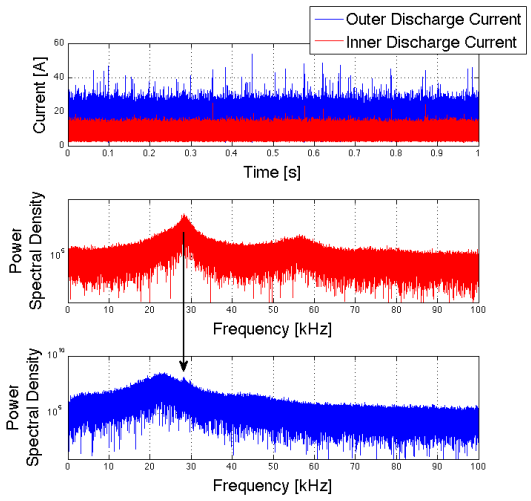

(d) 250 V

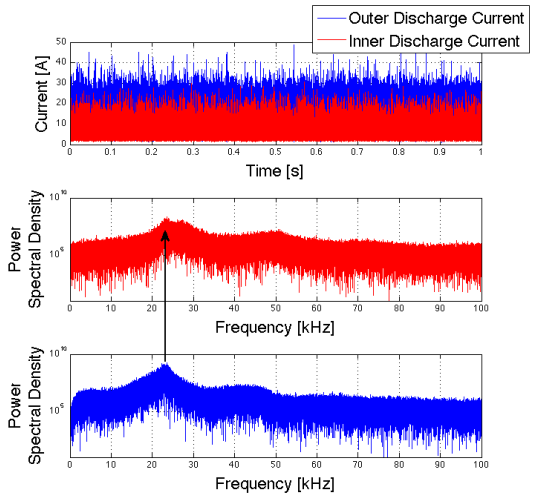

(e) 300 V

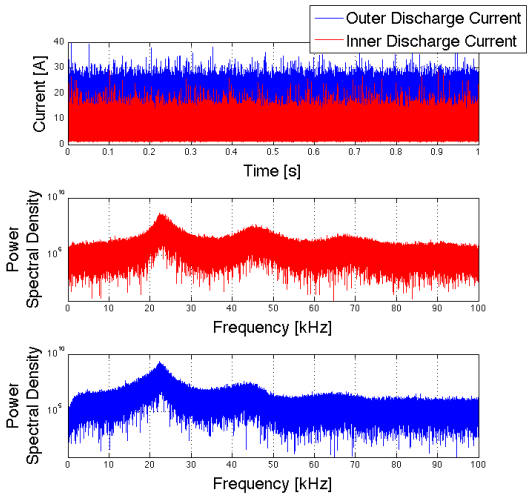

(f) 350 V

Figure 10: Discharge current measurements in dual-channel mode at 6 kW

measured and processed separately. The breathing mode frequencies, taken as the fundamental frequencies from the fast Fourier transforms, are shown in Figure 9(b).

$I_{d,AC}$, as a percentage of $I_{d,DC}$, reached a minimum at the two 200-V operating conditions. For dual-channel mode, the discharge current oscillations increased above and below 200 V as mass flow rate decreased and increased, respectively. The outer channel had discharge current oscillations of increasing strength from 200 V to 400 V as mass flow rate decreased, while the inner channel exhibited the same trend from 300 V to 600 V with decreasing flow rate.

For several dual-channel conditions, the Fourier transforms show oscillations at similar frequencies between both channels. At 125 V and 150 V, the two channels appear to be synchronized, although more harmonics were detected from the outer channel than the inner channel. Surprisingly, at 200 V, the two channels do not seem to interact in frequency space. Examination of the strength of the oscillations in Figure 9(a) shows that the 200 V operating condition is also the quietest. Small interactions are detected at 250 V and 300 V, where the fundamental frequency of one channel was detected in the discharge current of the other channel. This indicated some crosstalk between channels without complete synchronization of the current oscillations. At 350 V, $I_{d,AC}/I_{d,DC}$ is highest for all the 6-kW conditions, and the two channels are nearly synchronized again.

IV. Conclusion

The X2 NHT demonstrated constant-power operation at 5 kW and 6 kW between approximately 1080 s and 2860 s anode specific impulse. With three combinations of exit area, the X2 was able to transition between dual-channel mode and two single-channel modes in order to optimize performance and avoid the limitations of any one configuration. For constant-power operation, using nested channels simultaneously was most advantageous in the high thrust-to-power regime at low discharge voltages, where the increased mass flow capability was most needed. Single-channel operation at fixed power was best suited for moderate and high specific impulse.

RPA, E×B, and discharge current measurements provided additional insight into the characteristics of constant-power operation. Voltage utilization efficiencies increased with increasing discharge voltage and simultaneously decreasing mass flow rate. Charge utilization efficiencies remained within a 3% range with small variations between operating conditions. Discharge current measurements showed interactions between discharge channels in frequency space. Some synchronized operation was observed at low discharge voltages, while other forms of crosstalk was observed at higher voltages.

Acknowledgements

The authors would like to thank our sponsors, including Dr. Mitat Birkan at the Air Force Office of Scientific Research. This research was made possible through the Michigan/Air Force Center of Excellence in Electric Propulsion (MACEEP) and through Government support under and awarded by DoD, Air Force Office of Scientific Research, National Defense Science and Engineering Graduate (NDSEG) Fellowship, 32 CFR 168a for the first author. We would also like to thank the AFRL for the LaB_6 cathode and RPA used in our experiments. Thanks go to Adam Shabshelowitz and Roland Florenz for their assistance with experimental setup.

Appendix: Operation of the X2 on a Shared Power Supply

To determine if any crosstalk was due to the communication between discharge power supplies, the X2 was fired in dual-channel mode off the same discharge power supply. This was done prior to the 6-kW performance measurements shown previously and instead used one of the operating conditions from an existing throttle table. The discharge voltage applied to both channels was 150 V, and the mass flow rate combination was 9.3 mg/s through the inner channel and 23.3 mg/s through the outer channel. The cathode flow fraction was 10%, and the magnet settings were held constant. As shown in Figure 11(a) and 11(b) and Table 2, the discharge currents measured by the NT-series current sensors changed by only 1.2% for the inner channel and 0.5% for the outer channel. Breathing mode frequencies shifted by less than 1 kHz, and performance was nearly identical between power supply configurations. In Figure 11(a) and 11(b), an extra oscillation frequency corresponding to the outer channel's breathing mode appears on both FFTs of the inner discharge current. This form of crosstalk, which was also observed during 6-kW operation, is independent of the two power supply configurations.

Shared-power supply operation of an NHT also shows that such a thruster could operate on a single power processing unit (PPU). For the development of a flight model, shared-PPU operation of the nested channels could potentially

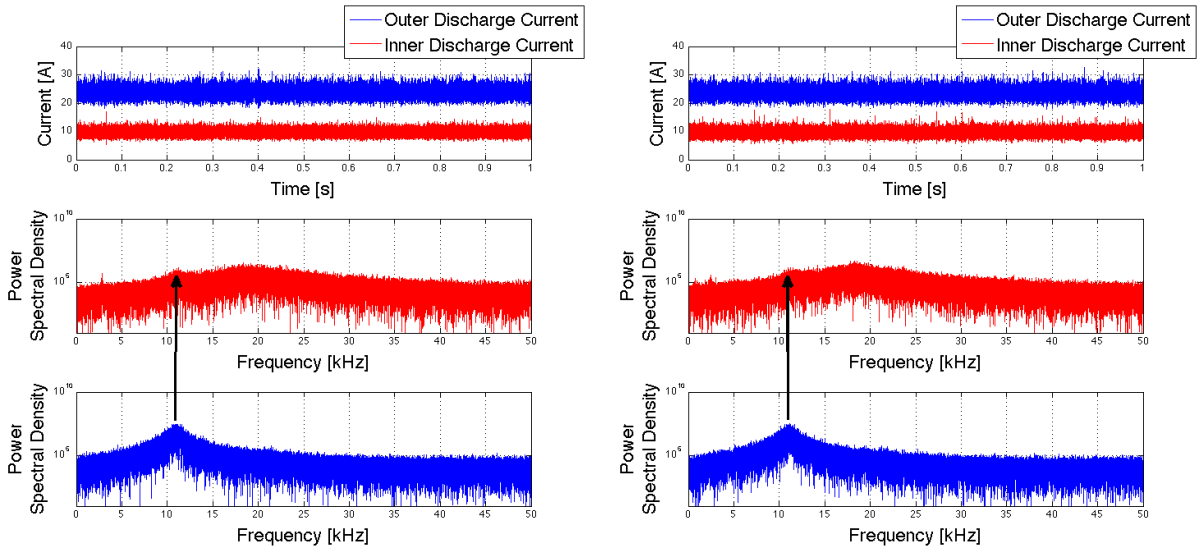

(a) Discharge current measurements for dual-channel operation with separate discharge power supplies

(b) Discharge current measurements for dual-channel operation with a shared discharge power supply

Figure 11: Comparison of dual-channel discharge characteristics with separate discharge power supplies and a shared discharge power supply

Table 2: Discharge and performance characteristics for operation with separate discharge power supplies and a shared discharge power supply

	Power Supplies	Power Supply
Discharge Voltage	150	150
Inner Discharge Current [A]	9.53	9.65
Outer Discharge Current [A]	23.65	23.77
Inner $I_{d,AC}/I_d$	11%	10%
Outer $I_{d,AC}/I_d$	7%	7%
Inner Breathing Mode Frequency [kHz]	18.6	19.3
Outer Breathing Mode Frequency [kHz]	11.0	10.9
Thrust [mN]	386	389
Anode Specific Impulse [s]	1211	1220
Anode Efficiency	46%	47%

simplify the implementation of an NHT. As the thrust, anode specific impulse, and anode efficiency did not vary significantly between power supply configurations, the use of a shared PPU is not expected to affect the performance of the thruster

References

[1]Jacobson, D.T., John, J.W., Kamhawi, H., Manzella, D.H, and Peterson, P.Y., "An Overview of Hall Thruster Development at NASA's John H. Glenn Research Center," *41st AIAA/ASME/SAE/ASEE Joint Propulsion Conference and Exhibit*, Tucson, AZ, July 2005, pp. 1–15.

[2]Brown, D.L., Beal, B.E., and Haas, J.M., "Air Force Research Laboratory High Power Electric Propulsion Technology Development," *IEEE Aerospace Conference*, Big Sky, MT, March 2010, pp. 1–9.

[3]Beal, B.E., *Clustering of Hall Effect Thrusters for High-Power Electric Propulsion Applications*, Ph.D. thesis, University of Michigan, Ann Arbor, MI, 2005.

[4]Walker, M.L.R. and Gallimore, A.D., "Performance Characteristics of a Cluster of 5-kW Laboratory Hall Thrusters," *Journal of Propulsion and Power*, Vol. 23, No. 1, 2007, pp. 35–43.

[5]Haag, T.W., "Thrust Stand for High-Power Electric Propulsion Devices," *Review of Scientific Instruments*, Vol. 62, No. 5, 1991, pp. 1186–1191.

[6]Reid, B.M., Shastry, R., Gallimore, A.D., and Hofer, R.R., "Angulary-Resolved E×B Probe Spectra in the Plume of a 6-kW Hall Thruster," *44th AIAA/ASME/SAE/ASEE Joint Propulsion Conference and Exhibit*, Hartford, CT, July 2008, pp. 1–21.

[7]Reid, B.M., *The Influence of Neutral Flow Rate in the Operation of Hall Thrusters*, Ph.D. thesis, University of Michigan, Ann Arbor, MI, 2009.

[8]Hofer, R.R., *Development and Characterization of High-Efficiency, High-Specific Impulse Xenon Hall Thrusters*, Ph.D. thesis, University of Michigan, Ann Arbor, MI, 2004.

[9]Varian, "Vacuum Measurement Catalog," 2010.

[10]Shastry, R., Hofer, R.R., Reid, B.M, and Gallimore, A.D., "Method for Analyzing E×B Probe Spectra from Hall Thruster Plumes," *Review of Scientific Instruments*, Vol. 80, No. 063502, 2009, pp. 1–11.

[11]Beal, B.E. and Gallimore, A.D., "Energy Analysis of a Hall Thruster Cluster," *28th International Electric Propulsion Conference*, Toulouse, France, March 2003, pp. 1–12.

[12]Liang, R. and Gallimore, A.D., "Far-Field Plume Measurements of a Nested-Channel Hall-Effect Thruster," *49th AIAA Aerospace Sciences Meeting*, Orlando, FL, January 2011, pp. 1–22.

[13]Hofer, R.R., "High-Specific Impulse Operation of the BPT-4000 Hall Thruster for NASA Science Missions," *46th AIAA/ASME/SAE/ASEE Joint Propulsion Conference and Exhibit*, Nashville, TN, July 2010, pp. 1–15.